Generation of primary photons through inverse Compton scattering using a Monte Carlo simulation code

Gianfranco Paternò,[1,2] Paolo Cardarelli,[2,*] Matteo Bianchini,[1] Angelo Taibi,[1,2] Illya Drebot,[3] Vittoria Petrillo,[4,3] and Ryoichi Hajima[5]

[1]*Department of Physics and Earth Science, University of Ferrara, via Saragat 1, 44122 Ferrara, Italy*
[2]*National Institute of Nuclear Physics (INFN) division of Ferrara, via Saragat 1, 44122 Ferrara, Italy*
[3]*National Institute of Nuclear Physics (INFN) division of Milano, via Celoria 16, 20133 Milano, Italy*
[4]*Department of Physics, University of Milano, via Celoria 16, 20133 Milano, Italy*
[5]*National Institutes for Quantum Science and Technology (QST), Tokai, Ibaraki 3191106, Japan*

(Received 31 March 2022; accepted 12 July 2022; published 24 August 2022)

Photon sources based on inverse Compton scattering, namely, the interaction between relativistic electrons and laser photons, are emerging as quasimonochromatic energy-tunable sources either as compact alternatives to synchrotron facilities for the production of low-energy (10–100 keV) x rays or to reach the 1–100 MeV photon energy range, which is inaccessible at synchrotrons. Different interaction layouts are possible for electron and laser beams, and several applications are being studied, ranging from fundamental research in nuclear physics to advanced x-ray imaging in the biomedical field, depending on the radiation energy range, intensity, and bandwidth. Regardless of the specific application, a reliable tool for the simulation of the radiation produced is essential for the design, the commissioning, and, subsequently, the study and optimization of this kind of source. Different computational tools have been developed for this task, based on both a purely analytical treatment and Monte Carlo simulation codes. Each of these tools has strengths and weaknesses. Here, we present a novel Monte Carlo code based on GEANT4 for the simulation of inverse Compton scattering in the linear regime. The code produces results in agreement with CAIN, one of the most used Monte Carlo tools, for a wide range of interaction conditions at a computational time reduced by 2 orders of magnitude. Furthermore, the developed tool can be easily embedded in a GEANT4 user application for the tracking of photons generated through inverse Compton scattering in a given experimental setup.

DOI: 10.1103/PhysRevAccelBeams.25.084601

I. INTRODUCTION

A. Inverse Compton sources

Inverse Compton scattering (ICS) is the process by which photons are scattered off relativistic electrons. As a result of the interaction, the scattered photons boost their energy, and it turns out to be correlated to the polar scattering angle. Typically, the colliding photons are those of intense laser pulses (visible or infrared light), and the electrons are accelerated in bunches. Since the energy of the backscattered photons scales linearly with the laser photon energy and quadratically with the electron energy, the emitted radiation can approach the x or gamma energy range with electron beam energies considerably smaller than those involved in synchrotrons. This feature allows one to design more compact accelerating machines [1]. Furthermore, the angle-energy correlation allows one to easily adjust the emitted radiation bandwidth by collimation. Finally, the intensity of the emitted radiation within a given collimation angle depends linearly on the charge of the electron bunches and the energy of the laser pulses [2]; thus, it can be improved as laser and acceleration technology advances.

For these reasons, ICS is one of the most promising methods for the realization of compact quasimonochromatic and energy-tunable photon sources. Many laboratories and research institutions worldwide have active projects for proof of principles, research, or user facility based on ICS, mainly for x-ray imaging applications in the 10–100 keV energy range [3–11] and nuclear physics research in the energy range 1–100 MeV and above [12–16].

Two different approaches are typically used for the implementation of an ICS source: an electron storage ring or an energy-recovery linac coupled to a laser resonator, such as a Fabry-Peŕot cavity, or a linear accelerator coupled to a low-repetition-rate high-peak-power laser system. Optionally, the latter can be equipped with a laser recirculator to match the laser repetition rate at the interaction

*cardarelli@fe.infn.it

point to that of the linear accelerator. As a result, the collision rate and, thus, the emitted photon flux can be increased.

An exhaustive treatment of the physical principles of ICS can be found in many specialized articles, such as Refs. [17–21]. As briefly described in the next subsection, the interaction between the electron and laser beams can occur at different regimes, depending on the electron energy and laser intensity. Generally speaking, the features of the produced radiation are all correlated among each other and strongly depend on the ones of the colliding beams and their collision conditions.

A reliable tool for the simulation and prediction of the emission characteristics is fundamental for the design and development of this kind of x-ray source, as well as for the operation diagnostics and optimization of the foreseen applications.

B. Overview of ICS simulation tools

The radiation emitted in the interaction between particles and electromagnetic fields has been analytically studied since the beginning of the last century. Thomson arrived through a pure classical electrodynamical treatment to the formulation of the cross section of the process, named the Thomson scattering cross section, this calculation being still now at the basis of most theoretical and numerical analyses [22].

X rays can be produced by taking advantage of the scattering process of laser photons off accelerated electrons. As mentioned at the beginning of this work, we generically call this process inverse Compton scattering.

Two important parameters help to classify the process, the first one being the dimensionless vector potential of the electromagnetic field $a_0 = eA/(mc\omega_L)$.[1] If $a_0 \ll 1$, the scattering is linear; i.e., the external electromagnetic field induces an electron purely harmonic motion. If, instead, a_0 is larger than 1, high harmonic modes develop in the oscillating trajectory of the electron, strongly affecting the radiation. The second parameter is the electron Lorentz factor γ. If the electrons are strongly energetic, quantum effects produce a recoil of the electrons during the interaction, shifting the radiation frequency. This is the Compton regime; otherwise, scattering events are said to occur in the Thomson regime. The simulation of x-ray radiation sources in the Thomson regime relies mainly on semianalytical codes, where the double differential spectral amplitude of the radiation emitted $d^2I/(d\Omega d\omega)$ with respect to frequency ω and solid angle Ω is evaluated for each electron through an analytical formula developed for the particular geometry of the system (see, for instance, Ref. [23]). The electron beam trajectories can be calculated analytically in the linear regime. In the nonlinear regime, the trajectories can be calculated numerically by using internal routines or by means of preexistent transport codes, such as PARMELA [24] or ELEGANT [25]. The sum over the electrons of the beam and the integration in angle and frequency is then done numerically. In this way, several numerical tools have been constructed. An example is the code developed for the source Pleiades at Lawrence Livermore National Laboratory [18,26], which can be used in the linear Thomson regime. Simulations in the nonlinear Thomson regime can be carried through $(TS)^2$ [27], which was used in the commissioning of the Thomson source SL_Thomson at INFN-LNF [11] or SENSE [28], which can handle chirped (frequency-modulated) pulses with an arbitrary envelope shape. In the linear Compton regime, ICCS [29] or ICARUS [30] can be used, the latter being based on the formalism introduced by Sun and coauthors [19,31]. Finally, the code described by Terzić and colleagues can be employed in the nonlinear Compton regime [32]. Codes based on the electrodynamical calculation of the double differential spectral amplitude permit taking into account the detailed structure of the electromagnetic external field (usually a laser), with temporal and transverse structure, polarization, phase modulations, and angular momentum [33]. They permit one to calculate not only the spectrum, but also the three-dimensional pattern of the complex electric field, allowing one to evaluate also advanced quantities as the output angular momentum or longitudinal and transverse coherence.

A different approach is to use the cross section of the process, that is at the bases of semianalytical or Monte Carlo codes. Usually, the Klein and Nishina [34] cross section is considered, permitting the exploration of the quantum linear or nonlinear regime. Semianalytical tools useful in the Compton linear regime are the ones described in Refs. [20,21]. CAIN, written by Yokoya *et al.* [35,36], is instead a stand-alone Monte Carlo program for the simulation of beam-beam interactions involving high-energy electrons, positrons, and photons. The laser amplitude is assigned as a Gaussian or doughnut power distribution, but the interaction is described as the scattering between particles. The code covers the linear and the weakly nonlinear regime in the classical and quantum domain and permits one to take into account features such as the collision angle, the multiple scattering, and the polarization of emitted photons. CAIN has been extensively tested and compared to experimental results (e.g., Ref. [19]), and it is often taken as a reference when new simulation codes are developed. Other Monte Carlo codes have recently become available, such as RF-Track [37], ROSE [38], or the one described in Ref. [39]. The latter two codes can be used in a full nonlinear regime. All the codes based

[1] e is the electron charge, m the electron mass, c the speed of light in vacuum, and A the vector potential of the field, and ω_L represents the field fundamental pulsation. For a laser, a_0 is also known as the strength parameter. A practical expression that correlates a_0 to the laser wavelength λ_L and intensity I is the following: $a_0 = 8.6 \times 10^{-9}\lambda_L(\mu\text{m})\sqrt{I(\text{W cm}^{-2})}$ [17].

on cross sections provide the power of the output radiation, without any information on the radiation phase. The Monte Carlo ones generally pack the electron beam into macroparticles during the simulation. Each macroparticle is represented by a certain number of real particles (the total number of particles in the beam divided by the number of macroparticles used in the simulation) sharing the same position, momentum, and energy. As a result, the output radiation is expressed as an ensemble of macrophotons. Therefore, the number of real photons emitted can be calculated only at the end of the process using the so-called "weight" of the macrophotons. Moreover, the macroparticle approach causes relative errors in the tail of the distributions much larger than the semianalytical one.

Notwithstanding some limitations, from the output provided by all the tools mentioned above, it is possible to obtain the phase space of x-ray emission through a proper postprocessing. This phase space can then be used as an input in other simulation codes devoted to radiation transport in matter, such as GEANT4 [40,41], MCNPX [42], EGSnrc [43], PENELOPE [44], or FLUKA [45], to carry out various tasks, such as the design of collimation systems, shielding, detectors, or to study and optimize the performance of various applications as a function of the ICS beam characteristics. Among these, GEANT4 is emerging as one of the most used particle-tracking codes in a large spectrum of research fields, spanning from high-energy physics to medical science, due to characteristics such as the fact that it is completely open source and fully exploits the potential of object-oriented programming, but also for its advanced geometry modeling, tracking algorithms, and high-accuracy physics models.

This work presents a tool that allows a user to include the generation of primary photons through linear ICS within a standard GEANT4 application, allowing one to directly study the source emission characteristics and the radiation transport in a specific experimental setup. The code is schematically described, and the comparison of the emission simulated with this code and the well-established CAIN tool is reported for three case studies of different ICS sources.

II. GEANT4 LASER COMPTON SCATTERING CODE

The code presented in this paper is based on the algorithm described in a previous work by Hajima [46] to simulate ICS in GEANT4. Such algorithm, referred to as LCS (which stands for laser Compton scattering), was developed with the aim of carrying out a specific task, namely, the optimization of collimators for Compton sources exploiting an electron beam with asymmetric emittance in the horizontal and vertical planes, such as those circulating in electron storage rings. For this reason, it has some limitations; the most significant is the handling of head-on beam-beam interactions only, since in a storage-ring-based ICS source this is the most common scenario [4,12,47]. Despite the reduction in the emitted flux, it may be convenient or necessary to consider optical cavities that foresee a nonzero crossing angle between the electron and laser beam. Indeed, a scheme with the laser optics out of the electron beam axis has been recognized as more convenient from alignment and operation points of view [48]. Moreover, it can be possible to envisage an interaction scheme of the electron beam with the laser at two different angles, so as to obtain a dual-energy beam [49], which can be exploited in various applications, in particular, medical ones [50,51]. Furthermore, depending on the optical cavity configuration, the laser profile at waist can be noncircular. For instance, a four-mirror (two flat and two curved) bow-tie cavity in the crossed configuration has been proposed [52] for the MariX/BriXS x-ray source, which is currently in the proposal stage [7,53]. Such a scheme guarantees a very high mechanical stability and allows one to match the cavity round-trip frequency to that of the electron beam and, at the same time, to control the laser beam waist. Because of the incidence angle on the curved mirrors of the cavity, the laser beam at waist has an elliptical profile with *a priori* non-negligible effects on the x-ray emission. Such a feature cannot be simulated with the original LCS code, which handles symmetrical laser beams only. Finally, in the original LCS implementation, the polarization of scattered photons is not evaluated.

In this work, we extended the original LCS algorithm to overcome its limitations and gain generality, so as to be able to simulate a variety of ICS sources in GEANT4. Here, we schematically describe the extended LCS code, highlighting the newly implemented features and the current limitations. In the next sections, we present three case studies used to compare the results provided by our code to those obtained with CAIN.

The original LCS algorithm was developed bearing in mind that the generation of primary photons in GEANT4 must be as simple and fast as possible, compatibly with the primary goal of catching the significant intrinsic properties of a Compton radiation source. Indeed, millions up to billions of primary photons are usually required in a realistic simulation. This principle inspired also this work; thus, we checked that the changes made did not significantly slow down the code. The code is based on the following assumptions on the colliding beams. (i) The incident beams have Gaussian distribution in their six-dimensional phase space of motion, but no correlation between the energy and the longitudinal coordinate. (ii) The laser is monochromatic. (iii) The laser is unpolarized or linearly polarized. (iv) The laser intensity is small, and nonlinear Compton scattering never occurs. (v) The incident beams collide so that the centers of pulses overlap at the design interaction point (IP) without any position or timing jitters.

The above assumptions are valid for a wide range of Compton radiation facilities, spanning from those based on electron storage rings such as high intensity gamma-ray

source [54] and NewSUBARU [15,55] to those based on electron linacs like BriXS [56], Southern Europe Thomoson back scattering source [8], BoCXS [5], or the Gamma beam system designed by EuroGammaS association for the extreme light infrastructure–nuclear physics facility [16]. Under these assumptions, ICS photons are generated as follows. (1) A point P is randomly sampled along the electron beam axis as the real interaction point. Point P is located within a range that includes the design collision point and is determined by the duration of the pulses and the envelopes of the colliding beams. (2) An electron is sampled from the six-dimensional electron beam phase space and transported to point P. (3) The product of the electron and laser photon density at point P is calculated considering that, in the case of non-head-on collisions, the nominal laser beam direction is tilted with respect to that of the electron beam. (4) A random sampling through the acceptance-rejection method according to the calculated density product, normalized by its maximum value, is carried out. (5) If the sampling is accepted, go to the next step. Otherwise, return to the first step. (6) The laser photon momentum is sampled taking into account the actual angle between the laser and the electron beam axis. (7) The sampled laser photon momentum is transformed so that it and the polarization vector are in the x-z plane of the laboratory frame with the electron moving along the z direction. (8) The laser photon momentum is transformed into the electron rest frame. (9) A scattered photon is generated at the electron rest frame, from the sampled electron and laser photon, according to the differential cross section of Compton scattering. (10) The scattered photon is transformed into the laboratory frame. (11) The scattered photon is accepted, provided that its momentum is within the collimator acceptance. (12) The polarization of the scattered photon is evaluated.

The sampling of scattered photons at the electron rest frame (step 9) is carried out by following the approach presented in detail in Ref. [19] and briefly in Ref. [46]; here, we describe it again in a more schematic way, which tightly represents the actual implementation of the algorithm.

The differential cross section of the Compton scattering process with respect to the energy of the scattered photon can be written as

$$\frac{d\sigma}{dE'_g} = \pi r_e^2 \frac{mc^2}{E'^2_p}\left(2 + \frac{2E'_p}{mc^2}\right) f(E'_g), \tag{1}$$

where m is the electron mass, c the speed of light in vacuum, E'_p the laser photon energy, E'_g the scattered photon energy, and

$$f(E'_g) = \frac{1}{2 + 2E'_p/mc^2}\left[\left(\frac{mc^2}{E'_p} - \frac{mc^2}{E'_g}\right)^2 + 2\left(\frac{mc^2}{E'_p} - \frac{mc^2}{E'_g}\right) + \frac{E'_p}{E'_g} + \frac{E'_g}{E'_p}\right]. \tag{2}$$

It holds that $0 \le f(E'_g) \le 1$ for any E'_g. The scattered photon energy can then be sampled by uniformly generating a random value of E'_g in the range

$$\frac{E'_p}{1 + 2E'_p/mc^2} \le E'_g \le E'_p \tag{3}$$

and a uniform random number r within the range from 0 to 1. If $r \le f(E'_g)$, E'_g is accepted; otherwise, it is discarded, and the sampling process is repeated.

Once the scattered photon energy has been determined, the polar scattering angle in the electron rest frame θ' can be calculated by solving the following equation:

$$\frac{1}{E'_g} = \frac{1}{E'_p} + \frac{1}{mc^2}(1 - \cos\,\theta'). \tag{4}$$

Finally, the azimuthal scattering angle in the electron rest frame ϕ' can be sampled according to the following double differential cross section [19] through the rejection method:

$$\frac{d^2\sigma}{dE'_g d\phi'} = \frac{mc^2 r_e^2}{2E'^2_p}\left\{[1 + P_t\,\cos(2\tau' - 2\phi')] \times \left[\left(\frac{mc^2}{E'_p} - \frac{mc^2}{E'_g}\right)^2 + 2\left(\frac{mc^2}{E'_p} - \frac{mc^2}{E'_g}\right)\right] + \frac{E'_p}{E'_g} + \frac{E'_g}{E'_p}\right\}, \tag{5}$$

where τ' is the azimuthal angle of the linear polarization direction of the incident photon defined in the electron rest frame. Note that the quantity P_t, the degree of linear polarization of the incident photon beam, is invariant under Lorentz transformations.

The scattered photon generated through the described procedure is then transformed into the laboratory frame, and a check is carried out to select only photons with polar angles in the laboratory frame θ within the collimator angular aperture. It is worth noting that no variance reduction techniques are adopted. As a consequence, each generated photon has unitary weight.

The final step of the extended algorithm is to evaluate the scattered photon polarization. In the current version of our code, this goal is achieved only approximately. In particular, based on the results shown in Ref. [57], the polarization of the laser photon is transferred to the scatter photon for scattering angles smaller than $1/\gamma$, where γ is the Lorentz factor of the electron beam. This, of course, is a rough approximation, but it is a simple method to account for polarization within an angular range that is significant for applications, avoiding dealing with complex calculations involving Stokes parameters.

The LCS algorithm described here was implemented in GEANT4, version 11.0. Three classes LCSGammaSource, LCSGammaSourceData, and LCSGammaSourceMessenger allow the user to define a Compton radiation source as a

primary particle source similarly to the built-in method of GEANT4. Indeed, provided that these classes have been included within the files of a custom application, the user has to create an instance of LCSGammaSource in the PrimaryGeneratorAction and call the LCSGammaSource::GeneratePrimaryVertex method to generate photons through inverse Compton scattering. The LCSGammaSourceData, which contains most of the data and methods required for the photon sampling, is created as a singleton when LCSGammaSource is instantiated. The LCSGammaSourceMessenger class allows the user to set the parameters of the colliding beams, and, thus, of the radiation source, from a command line or a macro file. A further feature of the new code is the estimation of the expected photon flux (photons per second), which is carried out by using the analytical expressions reported in Ref. [2], independently of the number of generated photons. To obtain the flux estimate, the user has to set the collision rate, electron bunch charge, and laser pulse energy. The implementation of LCS takes advantage of the extended version of the CLHEP library [58,59], the latest version of which has to be separately installed and linked during GEANT4 installation. This extension makes it possible to take advantage of GEANT4 well-established particle-tracking capabilities in complex geometries for the simulation of heterogeneous experimental setup and applications, without the need of additional software to generate the primary photon beam. The implemented code is fully compatible with the multithread environment supported by GEANT4. As discussed in Sec. V, the generation of primary photons through LCS is about 200 times faster than using CAIN.

```
/run/initialize

/run/setfilenamesave output

/lcsgs/ebeam/energy 43.3e6   #mean energy (eV)
/lcsgs/ebeam/espread 2.e-3   #relative spread (sigma)
/lcsgs/ebeam/emitx 1.5e-6    #x norm. emitt. (m*rad)
/lcsgs/ebeam/emity 1.5e-6    #y norm. emitt. (m*rad)
/lcsgs/ebeam/alphax 0.0015   #Twiss parameters
/lcsgs/ebeam/alphay 0.0021
/lcsgs/ebeam/betax 0.00814   #(m)
/lcsgs/ebeam/betay 0.00814   #(m)
/lcsgs/ebeam/sigmaz 4.e-4 m  #bunch length
/lcsgs/laser/wavelength 1.03e-6  #m
/lcsgs/laser/Zrx 0.01098        #x Rayleigh length (m)
/lcsgs/laser/Zry 0.01098        #y Rayleigh length (m)
/lcsgs/laser/sigmaz 6.e-4 m     #pulse length
/lcsgs/laser/polphi 0.5     #in units of PI (0->x, 0.5->y)
/lcsgs/laser/poldeg 1           #polarization degree
/lcsgs/collAngle 7              #collision angle (deg)
/lcsgs/collRate 1.              #collision rate (Hz)
/lcsgs/eBunchCharge 400.e-12  #(C)
/lcsgs/laserPulseE 0.01         #(J)
/lcsgs/solidangle 50.e-3        #thetamax (rad)
/lcsgs/position 0 0 0 cm
/lcsgs/zlim1 -0.01 m
/lcsgs/zlim2 0.01 m
/lcsgs/zcut 0.01
/lcsgs/list

/run/printProgress 100000
/run/beamOn 1000000
```

FIG. 1. Example of a macro file for the ICS application.

An application, called simply ICS, that embeds LCS classes was developed to produce the phase space of a given radiation source in a format that corresponds to that of CAIN. In such a way, it was possible to directly compare the results provided by the two codes. In Fig. 1, an example of a macro file for the ICS application is shown. It is possible to notice that the user can define the feature of the colliding beams, the collimation angle (through the /lcsgs/solidangle command), and some geometrical restrictions to the range where the actual collision points can be located (/lcsgs/zlim1, /lcsgs/zlim1, and /lcsgs/zcut commands). The command /lcsgs/list prints to screen a summary of the parameters set and the estimated flux of the source. We highlight that the code can be used to generate an arbitrary number of photons, which can be set by the user though the standard /run/beamOn command.

III. SIMULATION OF ICS RADIATION SOURCES

In order to assess the performance of the developed code, three case studies were selected to represent a variety of the interaction modality and beam parameters involved. The considered sources are listed below. (1) *BriXS*, which is a proposed source devoted to x-ray imaging in the energy range 10–100 keV and is based on an energy recovery linear accelerator coupled with a Fabry-Pérot cavity.—This scheme allows laser pulses with moderate intensity to interact with a moderate emittance electron beam at a very high repetition rate. As mentioned before, the linearly polarized laser stored in the cavity features an elliptical spatial distribution at the IP. The foreseen applications of the expected x-ray radiation include a dual energy modality based on a rapid switch of the interaction laser at two different angles [60]. Therefore, the correct evaluation of the energy distribution as a function of the interaction angle is fundamental. In our study, we simulated a configuration for the production of an x-ray beam with peak energy near to the iodine K edge (33.17 keV). (2) *Laser Compton source at NewSUBARU*, which is an operative user facility for nuclear physics and fundamental research, based on a 0.5–1.5 GeV electron storage ring [15].—Lasers with different wavelengths are used to obtain photon beams with energy spanning from 1 to 40 MeV. This source is characterized by high repetition rate head-on interactions of a nonpolarized laser having a large waist with an electron beam having large and asymmetrical values of emittance. In our case study, we set the parameters to obtain a medium energy (≈1.9 MeV) gamma beam as in Ref. [46]. (3) *EuroGammaS Gamma beam system (EGammaS-GBS)*, which was a high-energy (1–20 MeV) source to be installed

TABLE I. Features of the colliding beams for the three sources considered.

		BriXS	NewSUBARU	EGammaS-GBS
Electron beam				
Energy (MeV)	E_e	44.0	1000.0	529.8
Energy spread (%)	σ_{E_e}/E_e	0.2	0.1	0.044
Normalized emittance (mm mrad)	$\varepsilon_{n,x}$, $\varepsilon_{n,y}$	1.5, 1.5	10.0, 0.1	0.44, 0.44
Spot (rms) radius (μm)	$\sigma_{e,x}$, $\sigma_{e,y}$	15.0, 15.0	71.5, 7.1	17.2, 16.4
	α_x, α_y	0.0, 0.0	0.0, 0.0	0.56, 0.01
Twiss parameters	β_x, β_y	0.013, 0.013	1.0, 1.0	0.70, 0.63
	γ_x, γ_y	76.9, 76.9	1.0, 1.0	1.88, 1.59
Bunch charge (pC)	Q	200	500	250
Bunch length (μm)	$\sigma_{e,s}$	450	300	271
Laser beam				
Wavelength (μm)	λ	1.03	10.0	0.515
Pulse energy (J)	U	0.0075	1.0	0.2
Pulse (rms) duration (ps)	$\sigma_{L,t}$	2.0	1.0	1.5
Spot (rms) size (μm)	$\sigma_{L,x}$, $\sigma_{L,y}$	20, 40	892, 892	14, 14
Laser strength parameter	a_0	0.0076	0.0381	0.0457
Collision conditions				
Collision angle (deg)	α	7.0	0.0	8.0
Collision rate (Hz)	r	1×10^8	1×10^8	3.2×10^3

at the ELI-NP facility, mainly for nuclear physics research [16]. The source was based on a normal conduction linac and an optical recirculator, to increase the repetition rate of interactions between the accelerated electron bunches and a joule-class laser with short duration pulses (1.5 ps). Since the source was conceived to produce an intense, highly monochromatic gamma beam (relative $BW \leq 0.5\%$), the foreseen value of energy spread and emittance for the electron beam were very small as well as the collimator aperture [61]. For this source, we focused on the 10 MeV beam, so as to cover a broad range of photon energies, taking into account the three case studies considered.

A complete simulation with both CAIN and our GEANT4 code was carried out, using the parameters reported in Table I. For each case, the same number of uncollimated photons (about 10^7) was simulated with the two codes. The comparison of the obtained results was performed focusing on the following aspects: (i) energy distribution as a function of the collimation angle, (ii) spatial distribution of energy, and (iii) spatial distribution of intensity.

IV. RESULTS AND COMPARISON WITH CAIN SIMULATIONS

The most important point to consider when comparing two different simulation methods for inverse Compton scattering is the energy distribution of simulated photons as a function of the collimation angle. Indeed, if the two methods agree with each other and correctly reproduce the expected spectrum shape, it means that the simulation models are accurate enough to catch the fundamental relationships between the physical quantities involved in the process. In Figs. 2–4, the energy spectra for three simulated sources are reported considering three different collimations (one couple of curves refers to uncollimated spectra). It is possible to note that the general agreement is excellent, and a small discrepancy can be observed only in the simulations of the EGammaS-GBS. In particular, the low-energy cutoff of the collimated spectra simulated with our code is at a slightly lower energy if compared to the spectrum obtained with CAIN. A quantitative comparison was carried out by repeating ten times the simulations and calculating the mean value and the standard deviation of the most important spectral parameters, namely, the peak value E_p, the maximum value $E_{\max}$, the mean value E_m, and the relative bandwidth BW. Table II reports the calculated values for the narrower collimation angle. The tabulated

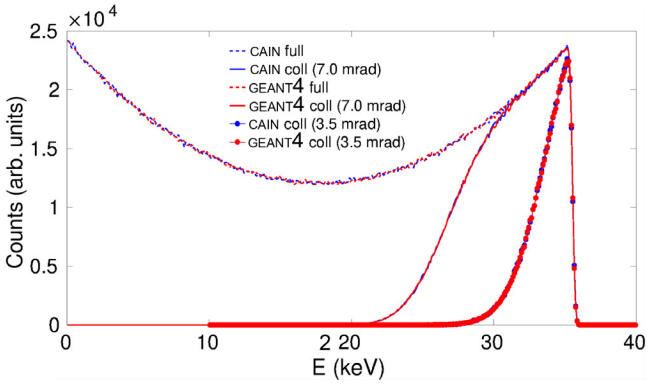

FIG. 2. Full and collimated spectrum of the BriXS photon beam simulated with CAIN and GEANT4.

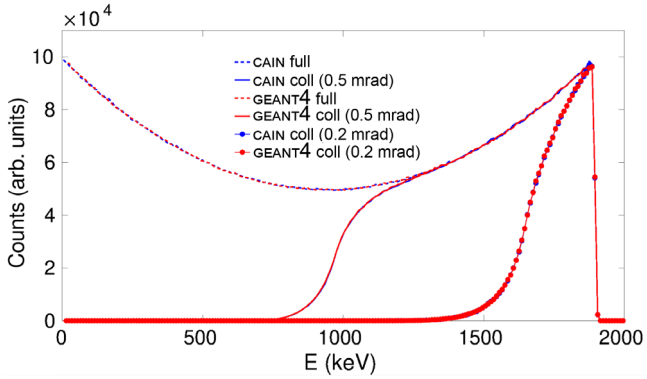

FIG. 3. Full and collimated spectrum of the NewSUBARU photon beam simulated with CAIN and GEANT4.

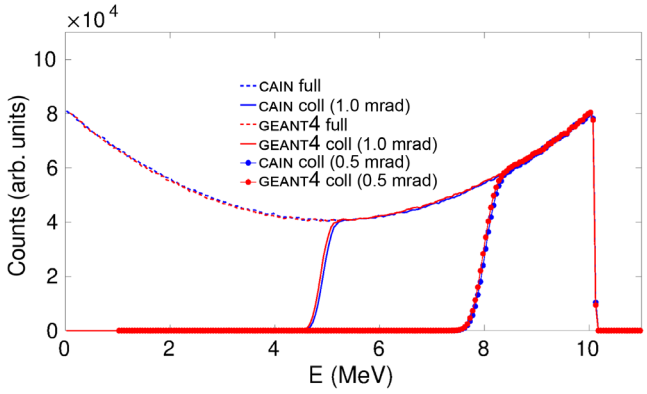

FIG. 4. Full and collimated spectrum of the EGammaS-GBS photon beam simulated with CAIN and GEANT4.

values confirm that the simulated spectra for the first two cases are fully compatible, while there is a slight discrepancy in the simulations of the third case, which is the one involving photons at higher energy. In particular, there exists a relative difference of 0.2% in the mean energy values and 1.5% in the energy bandwidth, respectively. On the other hand, it is important to note that the new implemented feature of allowing non-head-on interactions works well in our code, since in the simulations of BriXS and EGammaS-GBS sources the maximum beam energy is correctly reproduced with respect to CAIN. Therefore, the discrepancies in the mean value and bandwidth of the collimated beam spectra are due to the slight difference in the low-energy tail of the energy distribution.

A further proof of the perfect agreement between the simulations of the energy distribution for low- and mid-energy beams is shown in Fig. 5, where the energy distribution of scattered photons as a function of the polar scattering angle is plotted for the NewSUBARU source. The distributions simulated with the two codes are almost identical and follow the peculiar shape predicted by the theory. Furthermore, in Fig. 6, the spatial distribution of scattered photon energies at a fixed distance from the IP (10 m) is shown for the BriXS source. Also, in this low-energy case, the distributions obtained with CAIN and GEANT4 present the expected azimuthal symmetry and are indistinguishable.

We now focus on the compatibility assessment between the spatial distribution of the scattered photon beam intensity simulated with CAIN and GEANT4. Figures 7 and 8 show the spatial distribution of the scattered photon intensity (number of photons per bin) at a fixed distance from the IP (10 m) for NewSUBARU and EGammaS-GBS sources. The qualitative agreement is apparent, and the distributions reflect the polarization state of the laser, nonpolarized for NewSUBARU and linear polarized along the y axis for EGammaS-GBS, respectively. A more quantitative comparison can be obtained by analyzing the profiles of the spatial distribution along the transverse axes. As an example, we report, in Fig. 9, the profiles related to EGammaS-GBS source and, in Table III, the analysis of the relative differences (residuals) between the profiles obtained with CAIN and GEANT4. The maximum residual resulted smaller than 4%, and the correlation coefficient is very close to unity for both profiles. As a further analysis, we subtracted directly the spatial distributions obtained with the two simulation codes and made a binwise statistical analysis on the difference values for each of the three case studies. To avoid artifacts in the border due to a low statistics, for each source we considered only the

TABLE II. Comparison of the simulated photon beam with CAIN and GEANT4 for the three cases considered. The first set of features are related to collimated beams, while the second set refers to the whole source rms size at the IP.

	BriXS		NewSUBARU		EGammaS-GBS	
	CAIN	GEANT4	CAIN	GEANT4	CAIN	GEANT4
$\theta_{\max}$ (mrad)	3.5	3.5	0.2	0.2	0.5	0.5
E_m (keV)	33.70 ± 0.01	33.70 ± 0.01	1761.1 ± 0.3	1760.9 ± 0.3	9119 ± 1	9102 ± 1
BW (%)	4.32 ± 0.01	4.33 ± 0.02	5.63 ± 0.01	5.63 ± 0.02	6.76 ± 0.01	6.86 ± 0.01
E_p (keV)	35.19 ± 0.05	35.16 ± 0.07	1879 ± 5	1881 ± 5	10010 ± 34	10010 ± 41
$E_{\max}$ (keV)	36.01 ± 0.09	36.00 ± 0.05	1908 ± 2	1908 ± 2	10129 ± 2	10130 ± 4
$\sigma_{x,IP}$ (μm)	17.86 ± 0.07	10.49 ± 0.01	71.33 ± 0.04	50.46 ± 0.04	15.78 ± 0.01	11.96 ± 0.01
$\sigma_{y,\mathrm{IP}}$ (μm)	15.65 ± 0.08	10.24 ± 0.01	7.16 ± 0.01	5.06 ± 0.01	10.66 ± 0.01	8.93 ± 0.01
$\sigma_{z,\mathrm{IP}}$ (μm)	403.3 ± 0.4	240.5 ± 0.3	300.1 ± 0.2	211.4 ± 0.1	242.9 ± 0.2	149.0 ± 0.1

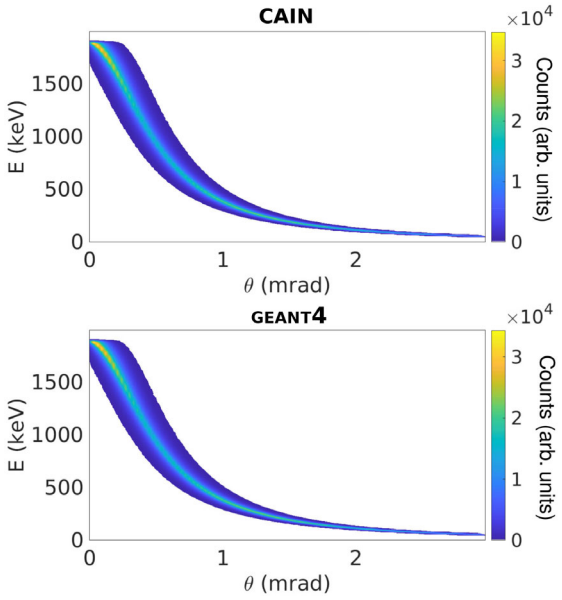

FIG. 5. Energy of emitted photons E versus polar emission angle θ for the NewSUBARU photon beam, simulated with CAIN and GEANT4.

photons within the collimation angle reported in Table I and adjusted the bin size to obtain enough counts on most of the bins. The mean value and the standard deviation of the calculated differences are reported in Table IV. In all the cases, the standard deviation of residuals was smaller than 10%, which is smaller than the statistical fluctuations.

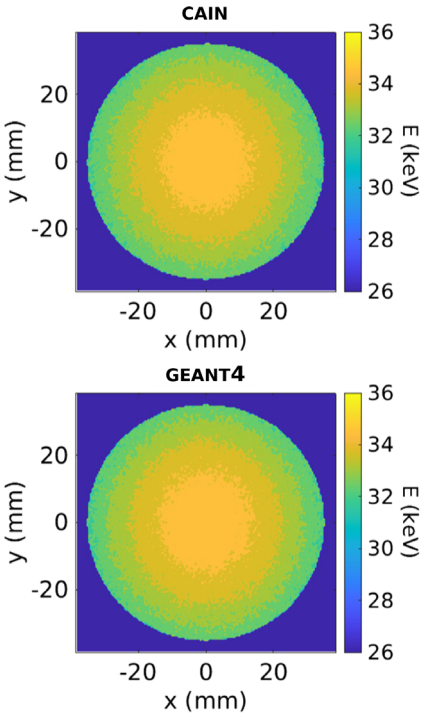

FIG. 6. Spatial distribution of energy at a distance from the IP of 10 m for the BriXS photon beam simulated with CAIN and GEANT4 within a collimation angle of 3.5 mrad.

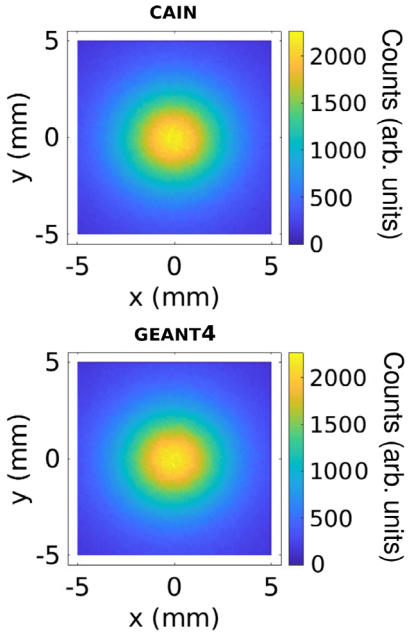

FIG. 7. Intensity spatial distribution at a distance from the IP of 10 m for the NewSUBARU photon beam simulated with CAIN and GEANT4. The axis scale was set to highlight the most significant part of the distribution.

The previous analysis mostly highlights the validity of the simulated beam divergence with respect to the traversal axes. Instead, if we focus on the beam spatial distribution at the IP, we find some discrepancies between the beam size obtained with CAIN and our GEANT4 code. As reported in

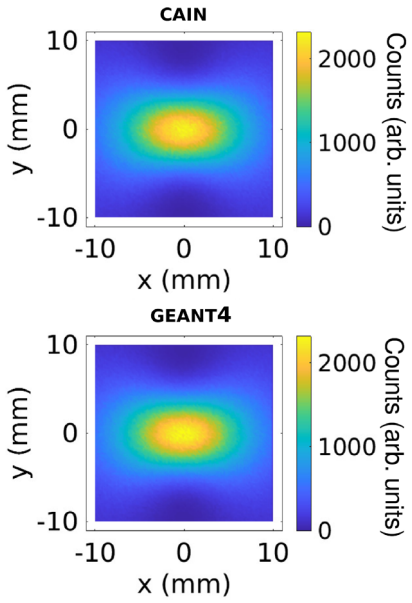

FIG. 8. Intensity spatial distribution at a distance from the IP of 10 m for the EGammaS-GBS photon beam simulated with CAIN and GEANT4. The axis scale was set to highlight the most significant part of the distribution.

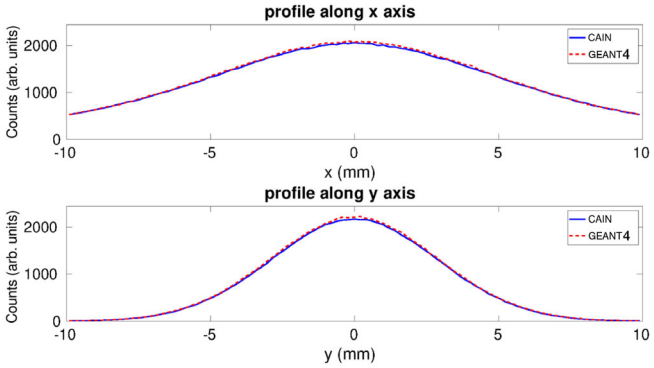

FIG. 9. Profiles of the intensity spatial distribution for the EGammaS-GBS photon beam simulated with CAIN and GEANT4. The axis scale is set so as to highlight the most significant part of the distribution.

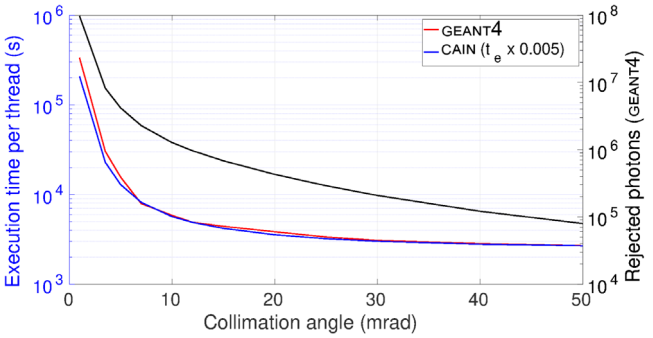

FIG. 10. Time (t_e) required to simulate 10^6 collimated photons with GEANT4 (blue curve) and CAIN (red curve), in the case of the BriXS source. The simulations were carried out on a server equipped with an Intel(R) Xeon(R) Gold 5220R CPU and 96 GB of RAM, and the reported execution times refer to single-thread mode. The number of rejected photons using the algorithm implemented in GEANT4 is also plotted (black curve).

Table II, our code produces always beams with smaller rms size with respect to CAIN.

Finally, we report the comparison of the simulation times between our GEANT4 code and CAIN. Figure 10 shows the time required to obtain 10^6 BriXS collimated photons with the two simulation codes as a function of the collimation angle. The curves feature almost the same behavior. The computation time dramatically increases as the collimation becomes narrower and narrower, but our code is about 200 times faster, since the curve related to CAIN is scaled by a factor of 0.005. It is worth noting that the plotted times are those required if only one thread is employed. In the case of multithreading, the reported times have to be reduced proportionally. The figure also plots the number of rejected photons to obtain the desired number of collimated photons with our code. As expected, the number of rejected photons increases as the acceptance angle tightens. The rejection rate becomes steeper for small collimation angles, and, as a result, the reject photons can be more than the generated ones.

TABLE III. Mean (Δ_{mean}) and maximum (Δ_{max}) value of the residuals calculated on the profiles shown in Fig. 9. Also, the correlation coefficient is reported.

Profile	Δ_{mean}	Δ_{max}	Correlation coefficient
Along x axis	1.4%	3.6%	0.9998
Along y axis	2.0%	3.9%	0.9999

TABLE IV. Analysis of binwise difference between the spatial distributions at 10 m from the IP of the collimated photon beams simulated with CAIN and GEANT4. The mean (Δ_{mean}) and the coefficient of variation (COV) of the residuals are reported.

Case	Δ_{mean}	COV	Collimation angle	Bin size
BriXS	0.01%	8.1%	3.5 mrad	1.43×1.43 mm^2
NewSUBARU	−0.1%	4.5%	0.2 mrad	0.08×0.08 mm^2
EGammaS-GBS	−1.8%	8.4%	0.5 mrad	0.10×0.10 mm^2

V. DISCUSSION AND CONCLUSIONS

In this paper, we presented a code for the simulation in GEANT4 of inverse Compton scattering events in the linear regime. The code is based on an algorithm presented recently by Hajima. Here, we describe the implemented extensions, which allow the user to simulate a significantly wider class of ICS sources and add useful information about the produced photon beams. In particular, the code is now capable of handling non-head-on interactions between the electron beam and the laser. Also, the laser shape at the interaction point can be now asymmetrical. Furthermore, a simple mechanism of laser polarization transfer to scatter photons was implemented. Finally, the simulation output includes now an estimation of the photon flux obtainable with the simulated ICS source.

The implemented code was described rather in detail and compared with CAIN code for three ICS sources featuring characteristics different from each other. The results provided by the two simulation tools are in excellent agreement. Some minor differences resulted in the spatial distributions of the simulated sources at the IP and in the energy distributions for the source with the higher energy. In the simulations of the photon beam spectra of EGammaS-GBS at 10 MeV, we found a relative difference of 0.2% in the mean values and 1.5% in the bandwidth, respectively. This effect is always present in the simulation of high-energy photon beams ($E_p \geq 2$ MeV) and becomes more apparent as the x-ray energy increases. Nonetheless, the discrepancies with CAIN are always of the order of a few percent and can be accepted for most of the applications, especially by virtue of the advantage in terms of computation speed guaranteed by our code, which resulted up to 200 times faster. In regard to the discrepancy in the spatial distributions of the simulated sources at the IP,

we think that this issue is not so relevant in practice, since the typical transverse size of an ICS source at the IP is very small (tens of micrometers) and the beam enlargement due to divergence dominates even at a short distance from the IP (tens of centimeters). On the other hand, the typical longitudinal size of an ICS source (from hundreds of micrometers to a few millimeters) is much smaller than the distance at which the irradiated object is positioned (from meters to tens of meters).

The use of our code can be twofold. It can be used as a stand-alone tool to study the emission characteristics of an ICS source for planning design and optimization, or it can be integrated in a user application for a start to end simulation of a photon beam line. Actually, it may be convenient from a computational point of view to split the simulation in two parts. In the first part, the required number of photons can be generated at the IP within a given acceptance angle and the obtained phase space saved to a .csv or root file [62]. In the second part, the generated photons can be read all at once and pushed in a stack through a dedicated class and then tracked one by one within the experimental setup. In this case, the overall simulation time may results significantly shorter (down to 4 times) with respect to the case in which each ICS photon is tracked just after its generation, due to better memory management. The user can in any case take advantage of the computation speed of our code and perform the whole simulation task using GEANT4. The only drawback is the requirement of storage for the generated phase-space file, which, on the other hand, would be the same if another code is used to generate it. The information about the flux foreseen for the considered ICS source can be useful for the normalization of the results obtained when the generated photons are tracked in a given experimental setup.

As future work, we plan to carry out further tests and benchmark the code against experiments. Also, we aim to mitigate the discrepancies with CAIN and refine the calculation of the scattered photon's polarization.

Finally, we remark that the developed code is freely downloadable [63].

ACKNOWLEDGMENTS

This work was carried out within the framework of MC-INFN and MariX_rad projects financed by INFN-CSN5. R. H. was supported by JSPS KAKENHI Grant No. 17H02818.

[1] R. Kuroda, Inverse Compton Scattering Sources, in *Comprehensive BioMedical Physics*, edited by A. Brahme (Elsevier, New York, 2014).

[2] C. Curatolo, I. Drebot, V. Petrillo, and L. Serafini, Analytical description of photon beam phase spaces in inverse Compton scattering sources, Phys. Rev. Accel. Beams **20**, 080701 (2017).

[3] K. Dupraz, M. Alkadi, M. Alves, L. Amoudry, D. Auguste, J.-L. Babigeon, M. Baltazar, A. Benoit, J. Bonis, J. Bonenfant *et al.*, The ThomX ICS source, Phys. Open **5**, 100051 (2020).

[4] B. Günther, R. Gradl, C. Jud, E. Eggl, J. Huang, S. Kulpe, K. Achterhold, B. Gleich, M. Dierolf, and F. Pfeiffer, The versatile x-ray beamline of the Munich Compact Light Source: Design, instrumentation and applications, J. Synchrotron Radiat. **27**, 1395 (2020).

[5] A. Bazzani, P. Cardarelli, G. Paternò, M. Placidi, A. Taibi, and G. Turchetti, BoCXS: A compact multidisciplinary x-ray source, Phys. Open **5**, 100036 (2020).

[6] P. Cardarelli, A. Bacci, R. Calandrino, F. Canella, R. Castriconi, S. Cialdi, A. Del Vecchio, F. di Franco, I. Drebot, M. Gambaccini *et al.*, BriXS, a new X-ray inverse Compton source for medical applications, Phys. Med. **77**, 127 (2020).

[7] L. Serafini, A. Bacci, A. Bellandi, M. Bertucci, M. Bolognesi, A. Bosotti, F. Broggi, R. Calandrino, F. Camera, F. Canella *et al.*, MariX, an advanced MHz-class repetition rate x-ray source for linear regime time-resolved spectroscopy and photon scattering, Nucl. Instrum. Methods Phys. Res., Sect. A **930**, 167 (2019).

[8] L. Faillace, R. Agostino, A. Bacci, R. Barberi, A. Bosotti, F. Broggi, P. Cardarelli, S. Cialdi, I. Drebot, V. Formoso *et al.*, Status of compact inverse Compton sources in Italy: BriXS and STAR, in *Advances in Laboratory-based X-Ray Sources, Optics, and Applications VII*, Vol. 11110 (International Society for Optics and Photonics, Bellingham, WA, 2019), p. 1111005.

[9] X. Stragier, P. Mutsaers, and O. Luiten, Smart* Light: A tabletop, high brilliance, monochromatic and tunable hard x-ray source for imaging and analysis, Microsc. Microanal. **24**, 310 (2018).

[10] C. Tang, W. Huang, R. Li, Y. Du, L. Yan, J. Shi, Q. Du, P. Yu, H. Chen, T. Du *et al.*, Tsinghua Thomson scattering x-ray source, Nucl. Instrum. Methods Phys. Res., Sect. A **608**, S70 (2009).

[11] C. Vaccarezza *et al.*, The SPARC_LAB Thomson source, Nucl. Instrum. Methods Phys. Res., Sect. A **829**, 237 (2016).

[12] C. R. Howell, M. W. Ahmed, A. Afanasev, D. Alesini, J. Annand, A. Aprahamian, D. Balabanski, S. Benson, A. Bernstein, C. Brune *et al.*, International workshop on next generation gamma-ray source, J. Phys. G **49**, 010502 (2021).

[13] T. S. Carman, V. Litveninko, J. Madey, C. Neuman, B. Norum, P. G. O'Shea, N. R. Roberson, C. Y. Scarlett, E. Schreiber, and H. R. Weller, The TUNL-FELL inverse Compton γ-ray source as a nuclear physics facility, Nucl. Instrum. Methods Phys. Res., Sect. A **378**, 1 (1996).

[14] D. Gibson, F. Albert, S. Anderson, S. Betts, M. Messerly, H. Phan, V. Semenov, M. Shverdin, A. Tremaine, F. Hartemann *et al.*, Design and operation of a tunable MeV-level Compton-scattering-based γ-ray source, Phys. Rev. Accel. Beams **13**, 070703 (2010).

[15] H. Utsunomiya, S. Hashimoto, and S. Miyamoto, The γ-ray beam-line at NewSUBARU, Nucl. Phys. News **25**, 25 (2015).

[16] O. Adriani, S. Albergo, D. Alesini, M. Anania, D. Angal-Kalinin, P. Antici, A. Bacci, R. Bedogni, M. Bellaveglia,

C. Biscari *et al.*, Technical design report EuroGammaS proposal for the ELI-NP Gamma beam system, arXiv: 1407.3669.

[17] E. Esarey, S. K. Ride, and P. Sprangle, Nonlinear Thomson scattering of intense laser pulses from beams and plasmas, Phys. Rev. E **48**, 3003 (1993).

[18] W. J. Brown and F. V. Hartemann, Three-dimensional time and frequency-domain theory of femtosecond x-ray pulse generation through Thomson scattering, Phys. Rev. Accel. Beams **7**, 060703 (2004).

[19] C. Sun and Y. K. Wu, Theoretical and simulation studies of characteristics of a Compton light source, Phys. Rev. Accel. Beams **14**, 044701 (2011).

[20] V. Petrillo, A. Bacci, R. B. A. Zinati, I. Chaikovska, C. Curatolo, M. Ferrario, C. Maroli, C. Ronsivalle, A. Rossi, L. Serafini *et al.*, Photon flux and spectrum of γ-rays Compton sources, Nucl. Instrum. Methods Phys. Res., Sect. A **693**, 109 (2012).

[21] G. A. Krafft, E. Johnson, K. Deitrick, B. Terzić, R. Kelmar, T. Hodges, W. Melnitchouk, and J. R. Delayen, Laser pulsing in linear Compton scattering, Phys. Rev. Accel. Beams **19**, 121302 (2016).

[22] J. J. Thomson, *The Corpuscular Theory of Matter* (Constable, London, 1907).

[23] J. D. Jackson, *Classical Electrodynamics* (American Association of Physics Teachers, College Park, MD, 1999), p. 670.

[24] L. M. Young and J. H. Billen, The particle tracking code Parmela, in *Proceedings of the 2003 Particle Accelerator Conference, Portland, OR* (IEEE, New York, 2003), Vol. 5, p. 3521.

[25] M. Borland, Elegant: A flexible SDDS-compliant code for accelerator simulation, 10.2172/761286 (2000).

[26] W. Brown, S. Anderson, C. Barty, S. Betts, R. Booth, J. Crane, R. Cross, D. Fittinghoff, D. Gibson, F. Hartemann *et al.*, Experimental characterization of an ultrafast Thomson scattering x-ray source with three-dimensional time and frequency-domain analysis, Phys. Rev. Accel. Beams **7**, 060702 (2004).

[27] P. Tomassini, A. Bacci, J. Cary, M. Ferrario, A. Giulietti, D. Giulietti, L. A. Gizzi, L. Labate, L. Serafini, V. Petrillo, and C. Vaccarezza, Linear and nonlinear Thomson scattering for advanced x-ray sources in PLASMONX, IEEE Trans. Plasma Sci. **36**, 1782 (2008).

[28] B. Terzić, A. Brown, I. Drebot, T. Hagerman, E. Johnson, G. Krafft, C. Maroli, V. Petrillo, and M. Ruijter, Improving performance of inverse Compton sources through laser chirping, Europhys. Lett. **126**, 12003 (2019).

[29] N. Ranjan, B. Terzić, G. Krafft, V. Petrillo, I. Drebot, and L. Serafini, Simulation of inverse Compton scattering and its implications on the scattered linewidth, Phys. Rev. Accel. Beams **21**, 030701 (2018).

[30] K. Deitrick, G. H. Hoffstaetter, C. Franck, B. D. Muratori, P. H. Williams, G. A. Krafft, and B. c. v. Terzić, J. Crone, and H. Owen, Intense monochromatic photons above 100 keV from an inverse Compton source, Phys. Rev. Accel. Beams **24**, 050701 (2021).

[31] C. Sun, J. Li, G. Rusev, A. Tonchev, and Y. Wu, Energy and energy spread measurements of an electron beam by Compton scattering method, Phys. Rev. Accel. Beams **12**, 062801 (2009).

[32] B. Terzić, J. McKaig, E. Johnson, T. Dharanikota, and G. A. Krafft, Laser chirping in inverse Compton sources at high electron beam energies and high laser intensities, Phys. Rev. Accel. Beams **24**, 094401 (2021).

[33] V. Petrillo, G. Dattoli, I. Drebot, and F. Nguyen, Compton Scattered X-Gamma Rays with Orbital Momentum, Phys. Rev. Lett. **117**, 123903 (2016).

[34] O. Klein and Y. Nishina, Über die streuung von strahlung durch freie elektronen nach der neuen relativistischen quantendynamik von dirac, Z. Phys. **52**, 853 (1929).

[35] P. Chen, G. Horton-Smith, T. Ohgaki, A. Weidemann, and K. Yokoya, CAIN: Conglomérat d'ABEL et d'Interactions Non-linéaires, Nucl. Instrum. Methods Phys. Res., Sect. A **355**, 107 (1995).

[36] K. Yokoya, User manual of CAIN, version 2.40, 2009.

[37] A. Latina, RF-Track reference manual, 2020.

[38] I. Drebot, A. Bacci, D. Micieli, E. Milotti, V. Petrillo, M. R. Conti, A. Rossi, E. Tassi, and L. Serafini, Study of photon-photon scattering events, Nucl. Instrum. Methods Phys. Res., Sect. A **865**, 9 (2017).

[39] Y.-F. Li, R. Shaisultanov, Y.-Y. Chen, F. Wan, K. Z. Hatsagortsyan, C. H. Keitel, and J.-X. Li, Polarized Ultrashort Brilliant Multi-GeV γ Rays via Single-Shot Laser-Electron Interaction, Phys. Rev. Lett. **124**, 014801 (2020).

[40] S. Agostinelli, J. Allison, K. Amako, J. Apostolakis, H. Araujo, P. Arce, M. Asai, D. Axen, S. Banerjee, G. Barrand *et al.*, GEANT4—A simulation toolkit, Nucl. Instrum. Methods Phys. Res., Sect. A **506**, 250 (2003).

[41] J. Allison, K. Amako, J. Apostolakis, P. Arce, M. A. M, T. Aso *et al.*, Recent developments in GEANT4, Nucl. Instrum. Methods Phys. Res., Sect. A **835**, 186 (2016).

[42] L. S. Waters, G. W. McKinney, J. W. Durkee, M. L. Fensin, J. S. Hendricks, M. R. James, R. C. Johns, and D. B. Pelowitz, The MCNPX Monte Carlo radiation transport code, AIP Conf. Proc. **896**, 81 (2007).

[43] I. Kawrakow and D. Rogers, The EGSnrc code system: Monte Carlo simulation of electron and photon transport, technical report, 2016.

[44] J. Baro, J. Sempau, J. Fernández-Varea, and F. Salvat, PENELOPE: An algorithm for Monte Carlo simulation of the penetration and energy loss of electrons and positrons in matter, Nucl. Instrum. Methods Phys. Res., Sect. B **100**, 31 (1995).

[45] G. Battistoni, F. Cerutti, A. Fasso, A. Ferrari, S. Muraro, J. Ranft, S. Roesler, and P. Sala, The FLUKA code: Description and benchmarking, AIP Conf. Proc. **896**, 31 (2007).

[46] R. Hajima, Bandwidth of a Compton radiation source with an electron beam of asymmetric emittance, Nucl. Instrum. Methods Phys. Res., Sect. A **985**, 164655 (2021).

[47] A. Variola, J. Haissinski, A. Loulergue, F. Zomer *et al.*, THOMX technical design report, 2014.

[48] A. Bacci, I. Drebot, L. Serafini, V. Torri, V. Petrillo, M. R. Conti, E. Puppin, D. Alesini, M. Bellaveglia, F. Bisesto *et al.*, Status of the STAR project, in *Proceedings of the 7th International Particle Accelerator Conference, IPAC 2016* (JACoW, Geneva, 2016), pp. 1747–1750.

[49] I. Drebot, V. Petrillo, and L. Serafini, Two-colour x-gamma ray inverse Compton back-scattering source, Europhys. Lett. **120**, 14002 (2017).

[50] G. Paternò, P. Cardarelli, M. Gambaccini, L. Serafini, V. Petrillo, I. Drebot, and A. Taibi, Inverse Compton radiation: A novel x-ray source for K-edge subtraction angiography?, Phys. Med. Biol. **64**, 185002 (2019).

[51] G. Paternò, P. Cardarelli, M. Gambaccini, and A. Taibi, Dual-energy x-ray medical imaging with inverse Compton sources: A simulation study, Crystals **10**, 834 (2020).

[52] I. Drebot, A. Bacci, A. Bosotti, F. Broggi, C. Curatolo, L. Faillace, D. Giannotti, D. Giove, P. Michelato, L. Monaco *et al.*, Optimisation study of the Fabry-Pérot optical cavity for the MARIX/BriXS Compton x-ray source, in *Proceedings of the International Particle Accelerator Conference IPAC2018, Vancouver, BC, Canada* (JACoW, Geneva, Switzerland, 2018), pp. 4192–4195, 10.18429/JACoW-IPAC2018-THPMF056.

[53] L. Serafini, A. Bacci, F. Broggi, A. Bosotti, S. Coelli, C. Curatolo, I. Drebot, L. Faillace, D. Giannotti, D. Giove *et al.*, The MariX source (multidisciplinary advanced research infrastructure with x-rays), in *Proceedings of the International Particle Accelerator Conference IPAC2018, Vancouver, BC, Canada* (JACoW, Geneva, 2018), pp. 4199–4202, 10.18429/JACoW-IPAC2018-THPMF058.

[54] H. R. Weller, M. W. Ahmed, H. Gao, W. Tornow, Y. K. Wu, M. Gai, and R. Miskimen, Research opportunities at the upgraded HIγS facility, Prog. Part. Nucl. Phys. **62**, 257 (2009).

[55] K. Horikawa, S. Miyamoto, S. Amano, and T. Mochizuki, Measurements for the energy and flux of laser Compton scattering γ-ray photons generated in an electron storage ring: NewSUBARU, Nucl. Instrum. Methods Phys. Res., Sect. A **618**, 209 (2010).

[56] I. Drebot, A. Bacci, A. Bosotti, F. Broggi, F. Canella, P. Cardarelli, S. Cialdi, L. Faillace, G. Galzerano, M. Gambaccini *et al.*, BriXs ultra high flux inverse Compton source based on modified push-pull energy recovery linacs, Instruments **3**, 49 (2019).

[57] V. Petrillo, A. Bacci, C. Curatolo, I. Drebot, A. Giribono, C. Maroli, A. Rossi, L. Serafini, P. Tomassini, C. Vaccarezza *et al.*, Polarization of x-gamma radiation produced by a Thomson and Compton inverse scattering, Phys. Rev. Accel. Beams **18**, 110701 (2015).

[58] CLHEP—A class library for high energy physics, https://proj-clhep.web.cern.ch/proj-clhep/.

[59] L. Lönnblad, CLHEP—A project for designing a C++ class library for high energy physics, Comput. Phys. Commun. **84**, 307 (1994).

[60] I. Drebot, D. Giannotti, L. Serafini, S. Cialdi, V. Petrillo, P. Cardarelli, M. Gambaccini, G. Paternó, A. Taibi, I. R. Calandrino, A. Delvecchio, and G. Galzerano, Multi colour x-Gamma ray inverse Compton back-scattering source, in *Proceedings of the International Particle Accelerator Conference IPAC2018, Vancouver, BC, Canada* (JACoW, Geneva, 2018), pp. 4196–4198, 10.18429/JACoW-IPAC2018-THPMF057.

[61] G. Paternó, P. Cardarelli, M. Marziani, E. Bagli, F. Evangelisti, M. Andreotti, M. Gambaccini, V. Petrillo, I. Drebot, A. Bacci *et al.*, A collimation system for ELI-NP Gamma beam system—Design and simulation of performance, Nucl. Instrum. Methods Phys. Res., Sect. B **402**, 349 (2017).

[62] I. Antcheva, M. Ballintijn, B. Bellenot, M. Biskup, R. Brun, N. Buncic, P. Canal, D. Casadei, O. Couet, V. Fine *et al.*, ROOT—A C++ framework for petabyte data storage, statistical analysis and visualization, Comput. Phys. Commun. **182**, 1384 (2011).

[63] https://www.fe.infn.it/medical_physics/.